UNIVERSITY OF CALIFORNIA
RIVERSIDE

Microwoven Mesh Used for Particle Separation and Capture

A Thesis submitted in partial satisfaction
of the requirements for the degree of

Master of Science

in

Bioengineering

by

Astha Arora

December 2016

Thesis Committee:

Dr. William H. Grover, Chairperson
Dr. B. Hyle Park
Dr. Masaru P. Rao

The Thesis of Astha Arora is approved:

_____

_____

_____

Committee Chairperson

University of California, Riverside

TABLE OF CONTENTS

LIST OF FIGURES

1.INTRODUCTION

Cell separation is a powerful tool which is widely used in many fields of biological and biomedical research and clinical therapy.[1] A multitude of cell separation techniques currently available to researchers are based on four core themes: cell density, size, adherence and antibody binding, with many points of crossover between these different themes.[2] Clinical analysis usually requires the separation of cells from plasma or separate different types of cells . This type separation is mainly conducted through centrifugation, an old and tested method for cell sorting.

Since centrifugation requires a large and expensive instrument and usually requires trained personnel for operation, eliminating it would significantly reduce the expense of medical research and diagnostics. We aim to design a device for cell sorting and capture which is low cost, disposable, and easy to manufacture. For this, a great alternative to centrifugation could be the utilization of microfluidics for cell sorting. A continuous-flow device would make isolating cells of interest a fast and efficient process.

Furthermore, using centrifugation to separate circulating tumor cells (CTCs) is difficult because CTCs are rare (estimated to be 1 tumor cell to 1 billion healthy cells in circulation) and difficult to isolate. This greatly increases the need for a precise and high-throughput device to isolate circulating tumor cells.[9] Many microfluidic deterministic lateral displacement (DLD) devices are now being used for cell sorting and are efficient, but they still have drawbacks like high manufacturing cost and complex fabrication techniques.

Because of this, these technologies are still not widely applied for clinical uses. Therefore, our aim is to use the concepts of DLD in developing a feasible and efficient device for cell sorting and capture.

2. BACKGROUND

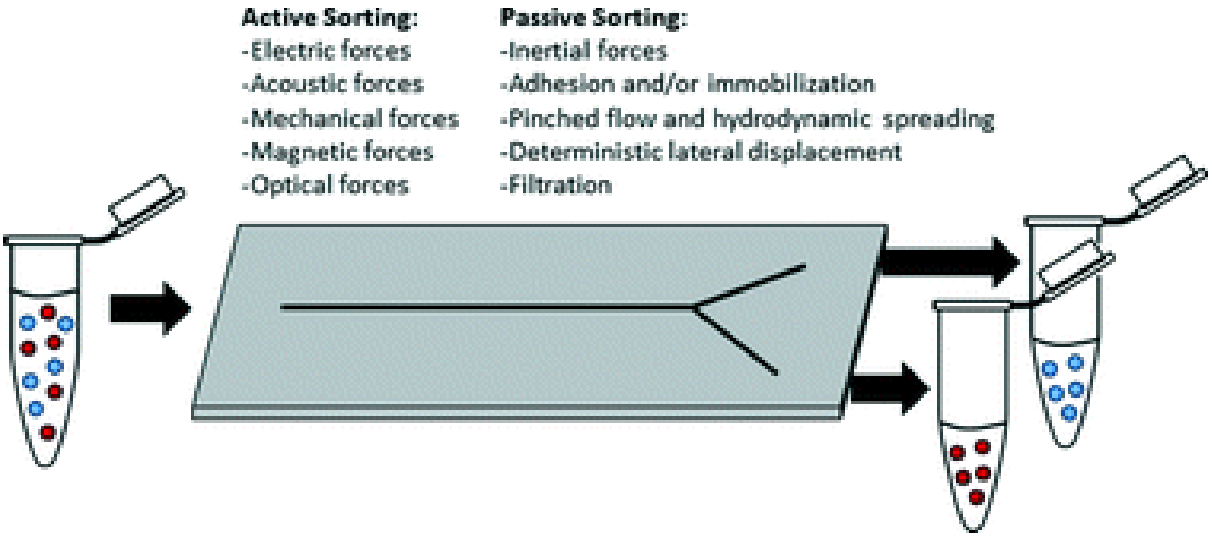

Figure 1: Types of Active And Passive Sorting

At present there are mainly two main methods of cell sorting: active and passive separation.

2.1 Active Separation:

This type of requires cells to be sorted based on external forces like optical forces, electric forces, magnetic forces, mechanical forces, etc. Figure 3 shows the use of magnetic force for the separation of CTC. In Figure 2A magnetic beads conjugated with anti-EpCAM are shown to capture and isolate CTCs under free flow in a magnetic field. Magnetically

labeled CTCs and leukocytes are filtered from blood via deterministic lateral displacement, focused via inertial focusing and sorted in a magnetic field.

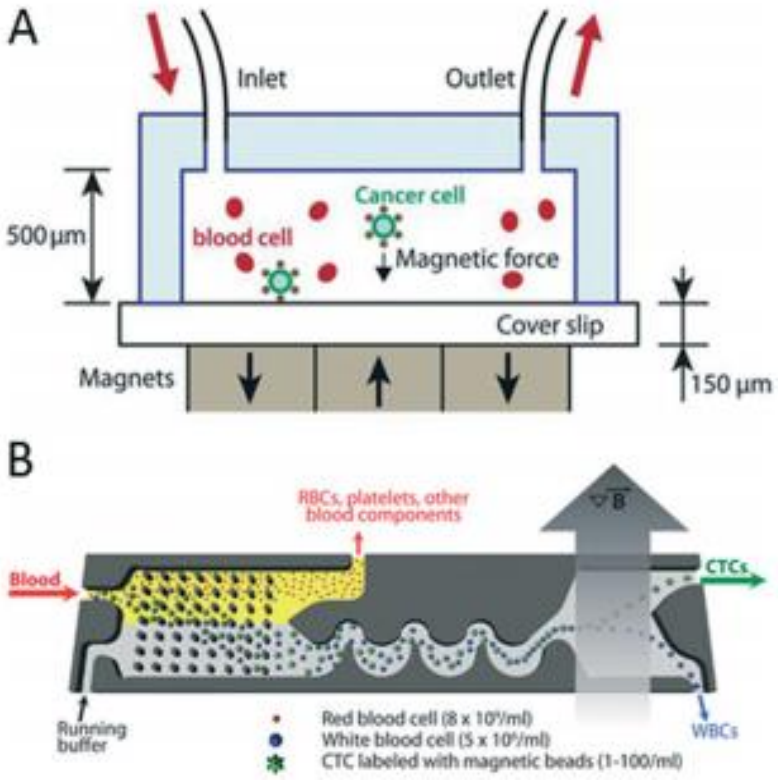

Figure 2: Type of Magnetic sorting. [10]

2.2 Passive Separation:

These methods generally use inherent differences of cell morphology like the size, density, compressibility. This type of separation uses technologies that do not usually rely on fluorescent labels or beads. Forces like cellular adhesion, deterministic lateral displacement (DLD) can be used for cell sorting. Figure 3 shows cell sorting by pinched flow fractionation.

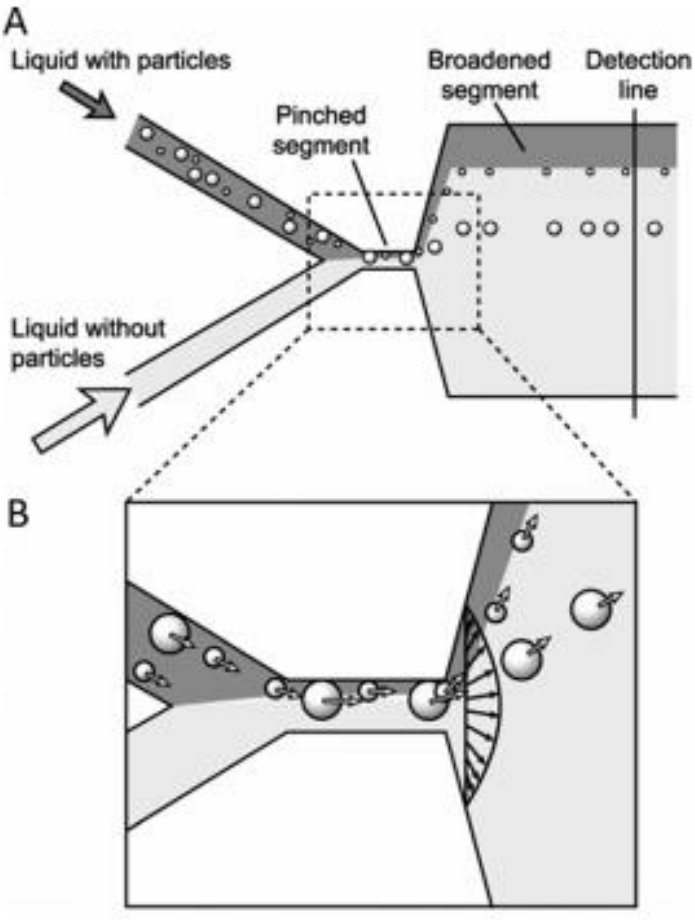

Figure 3: Pinched flow fractionation. A) In the pinched segment, cells are first pushed against the wall, and then separated by size upon broadening of the microfluidic channel. B) Cells are aligned in the Pinched segment of the channel and follow separate streamlines for sorting by size after exiting the pinched segment.[10]

The work in this thesis is mainly based on passive separation, where we use the concept of deterministic lateral development (DLD) for cell separation.

2.2.1:Deterministic Lateral Displacement Devices

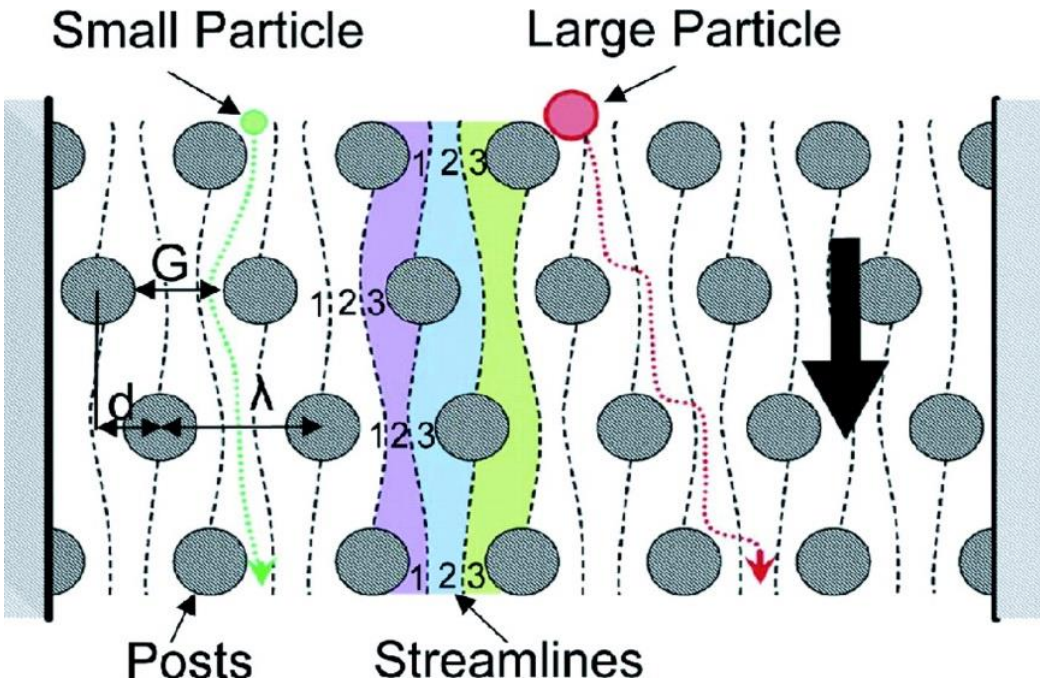

Figure 4: Deterministic lateral displacement device with an array of microposts that forms three different flow lamina through the device. The paths followed through the device by a small (green) and large (red) particle are shown [4][9].

In the example in Figure 4, the deterministic lateral displacement technique is performed using an array of microposts with a row shift fraction of one-third. This shift creates three equal flux streamlines. The shifting of the array can create multiple but consistent flow lamina through the device. The principle behind DLD is that a particle flowing through a lamina will continue to flow through that same flow lamina for the duration of the device if its center of mass remains within the flow lamina. [4]

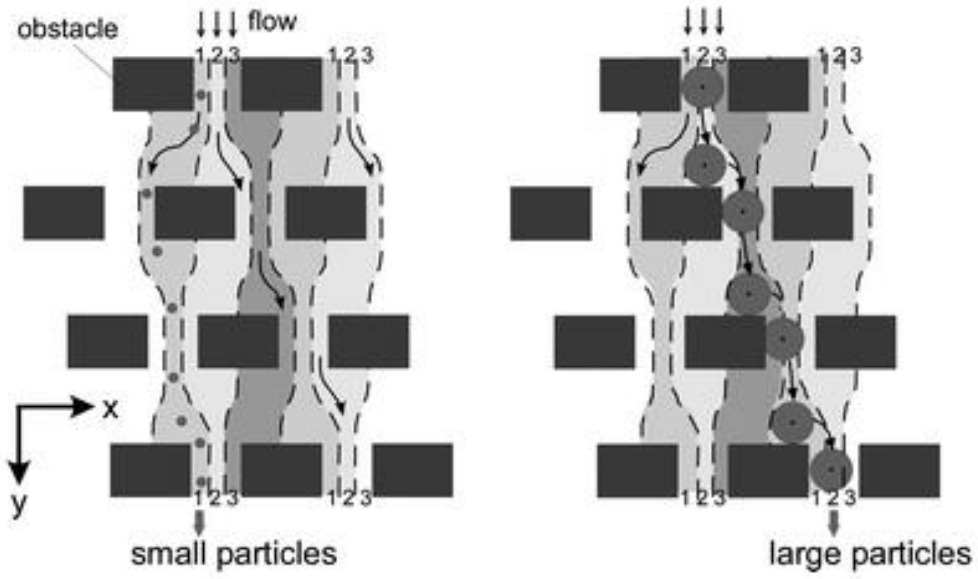

Figure 5: Another example of a DLD device with a post array, showing different flow lamina and the paths followed by two different-sized particles through the post array [4].

Figures 4 and 5 show that the separation two different sizes of cells in a DLD device. If a small particle has a center of mass located within a lamina, then the particle will continue to flow in the same lamina. The particle will tend to move in a zigzag way, without any net lateral displacement. However, if the size of a larger particle causes its center of mass to shift into an adjacent lamina, this phenomenon will continue throughout the device and force the larger particle to be displaced along the angle of the array.

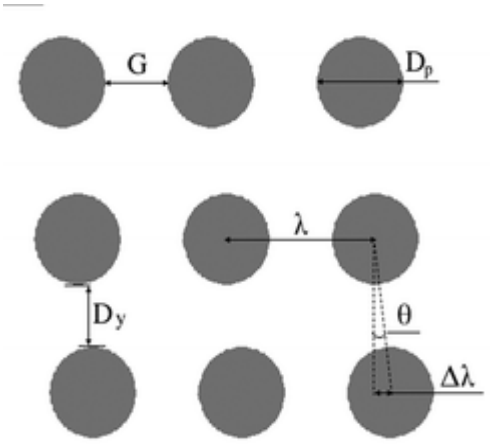

Figure 6: An illustration of a DLD post array, with key measurements needed for calculating the flow lamina and critical diameter.

There are a few factors that have to be taken into consideration for the particles to be sorted [9]. The parallel flow in a DLD chip is determined by the Reynolds Number (Re) which is less than one. At Re < 1, viscous forces are dominant and not the continuous forces. The diameter of the posts (Dp), as shown in figure 6, distance between the posts, and the angle at which the posts are shifted are used to determine what particles can be separated using a given device. The angle θ develops because of lateral row shifting and represents the alignment of each column relative to flow direction. When the posts of row N + 1 are in the same lateral position as the first row, the period is said to be N, which is also related to λ and Δλ:[9]

$$N = \frac{\lambda}{\Delta\lambda} \qquad (1)$$

$$\varepsilon = \frac{\Delta\lambda}{\lambda} = \frac{1}{N} = tan\theta \qquad (2)$$

$$D_C = 1.4G\varepsilon^{0.48} \qquad (3)$$

The ratio of the distance between the center of neighboring post, represented by λ (figure 6), and the distance of the center to center shift represented by Δλ with gives the number of laminas flowing between each post as shown by Equation (1). The row shift fraction (Ɛ) can be calculated by taking the inverse of the flow laminas or by taking the tangent of the shift angle θ as seen in Equation (2). The row shift fraction is then used to get the **critical diameter** D_C using Equation (3) which defines the critical diameter at which a particle with exhibit deterministic lateral displacement. [5][9]

2.2.2: Drawbacks of Current Devices:

There is now an large variety of continuous-flow cell separation devices but they are still rarely used clinically. An explanation for this could be that the time and complexity of fabricating these devices outweighs the benefits of the devices.[9] Also, the equipment required to microfabricate these devices can be very expensive. Consequently, these DLD devices are largely unsuitable for disposable use in a point-of-care setting.[9]

3. Results

In this work we developed a low-cost and disposable device using a commercially available woven mesh and applying the concepts of based on microfluidics; which can be used to separate and capture particles and cells based on their sizes.

3.1 Microwoven Mesh

We hypothesize that the principles that are applied cell sorting in DLD devices, can be very effective and competent for developing this device, by using lateral flow through a microwoven mesh. An advantage of commercially-available mesh is that it has a uniform micron-sized pattern, which in turn helps in calculating trajectories and flow in the mesh, as we would do in a DLD device.

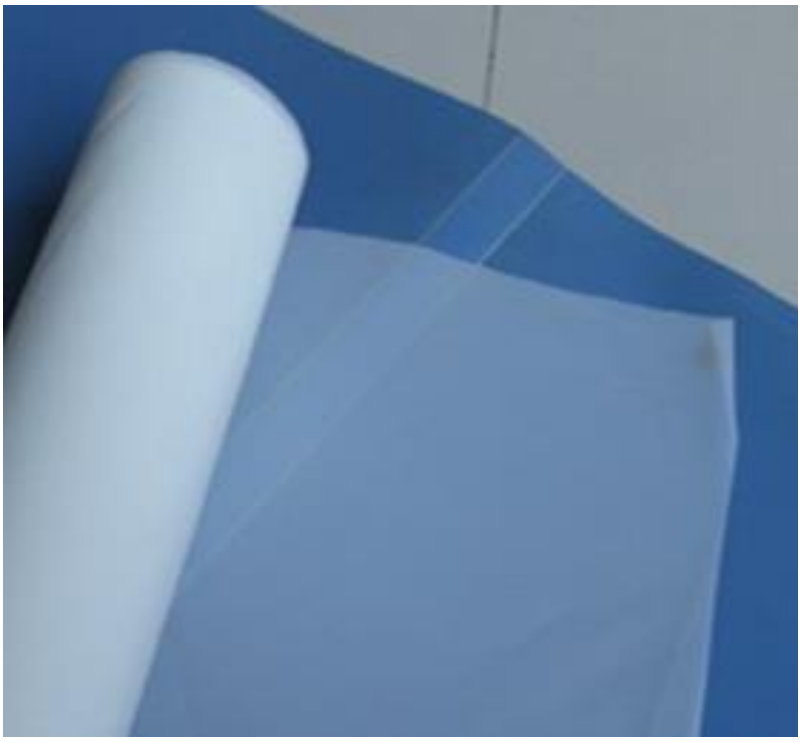

Figure 7: Photograph of microwoven mesh used in this project.

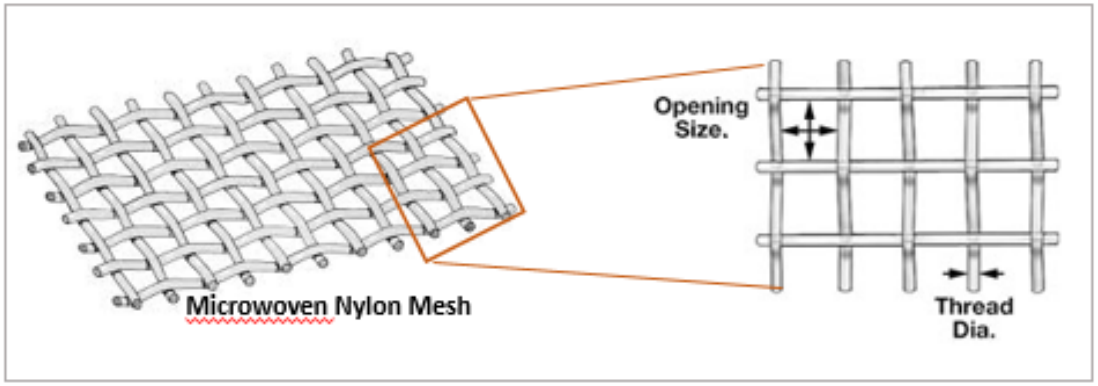

Figure 8: Illustration of mesh, showing the pore/opening size and the thread diameter.

There are various types and different materials of mesh that are commercially available. We decided to work with nylon and concentrated our work with a mesh opening size of 53 µm and 78 µm as particles with diameters 5 µm and 10 µm tend to interact with this mesh in a manner that resembles particles in a DLD device.

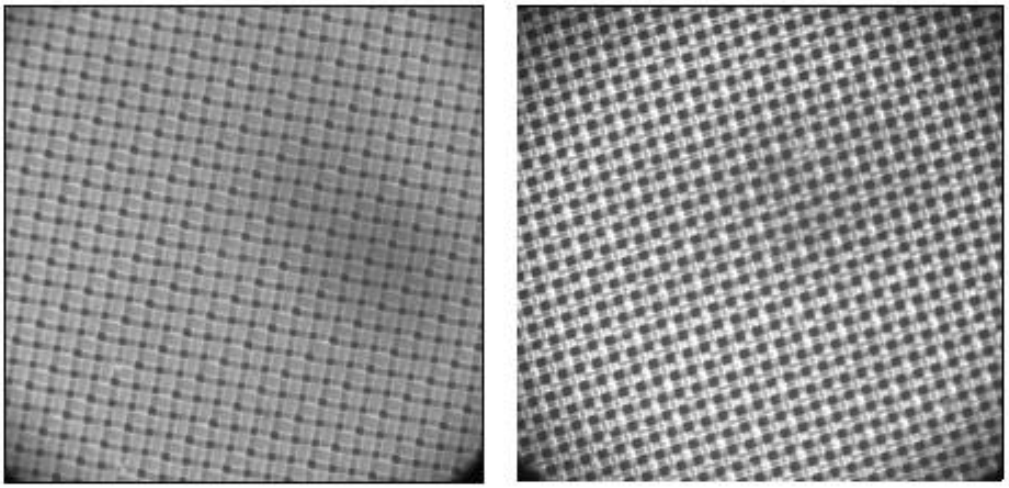

Figure 9: Micrographs of microwoven nylon mesh with opening sizes 50 μm and 78 μm. The 50 μm mesh has a thread diameter of 33 μm while 78 μm mesh has a thread diameter of 50 μm.

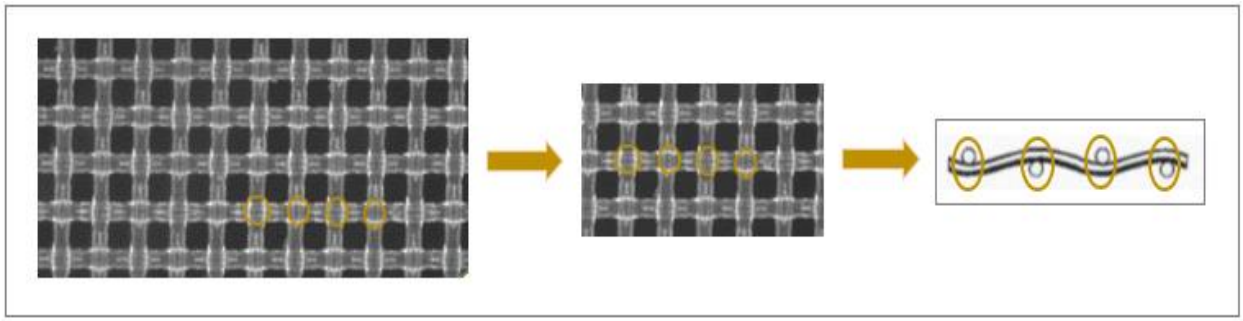

Figure 10: Micrograph of 78 μm nylon mesh, showing the alternating pattern of over-and-under features in the woven mesh.

Figure 10 shows the 78 μm nylon mesh under a microscope. The yellow circles represents the over-under overlap of the threads of the mesh. These features act as pillars or obstacles for the particles flowing through the mesh. We hypothesize that a precise arrangement of this type of mesh can help in sorting, as arranging them in particular angles will cause

particles of various sizes to behave differently as they flow laterally through the mesh in a manner akin to deterministic lateral displacement.

3.2 Device Design :

The first aim of this research is to continue exploring the possiblities of achieveing bump-array-like particle sorting using commercially-available meshes. Unlike existing DLD devices, the over-under nature of woven mesh gives the particles potentially a dense array of structure with which they can interact. This research focuses only on the Rigid Flow-through Device (Figure 11) .

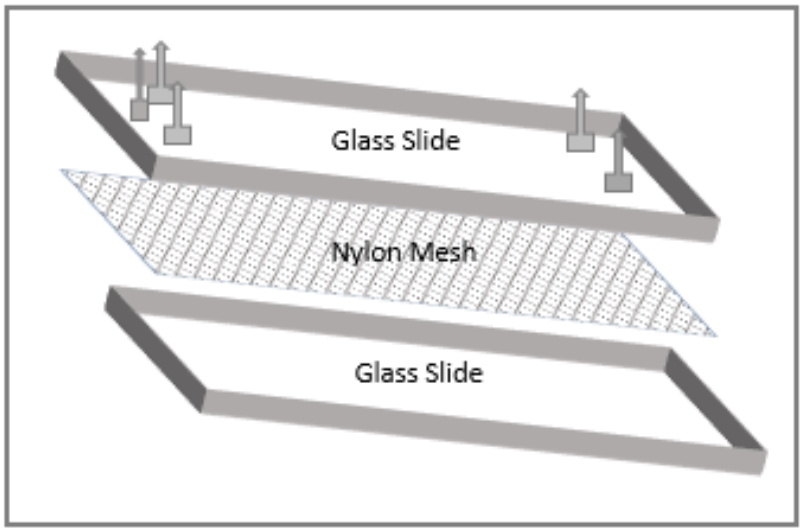

Figure 11: Schematic of Rigid Flow-through Device with three inlets, two outlets, and mesh placed between two glass slides.

A piece of mesh is cut to the size and shape of a glass slides. The mesh is placed between two glass slides that are subsequently glued together using epoxy on all four sides. The upper glass contains drilled holes that allow the flow of fluid into and out of the mesh. By attaching tubing adapters to these holes, we can control the flow rate and pressure of fluid entering the mesh. It also allows for us to continously monitor the amount and speed of fluid coming out of the outlet adapters.

Since the mesh is sandwiched between the slides, the mesh can be oriented at any angle. We can also use different types of meshes, as long as they can be properly sealed between the slides. Multiple uses of the same device can lead to leaking along the edges due to epoxy wear. Thus, every device is used only once not only to maintain the efficiency of the deivce but also to prevent any kind of wear.

A major advantage of this device is that is very inexpensive and easy to manufacture. A classic bump-array device requires a long process of microfabrication utilizing steps like deep reactive ion etching (DRIE). Multiple photomasks and photolithography steps are usually required to create the different channel heights in the DLD devices. In contrast, the microwoven mesh itself forms the microchannels and pillars in our devices, which makes it relatively easy and inexpensive to manufacture these devices.

3.3 Flow Visualization

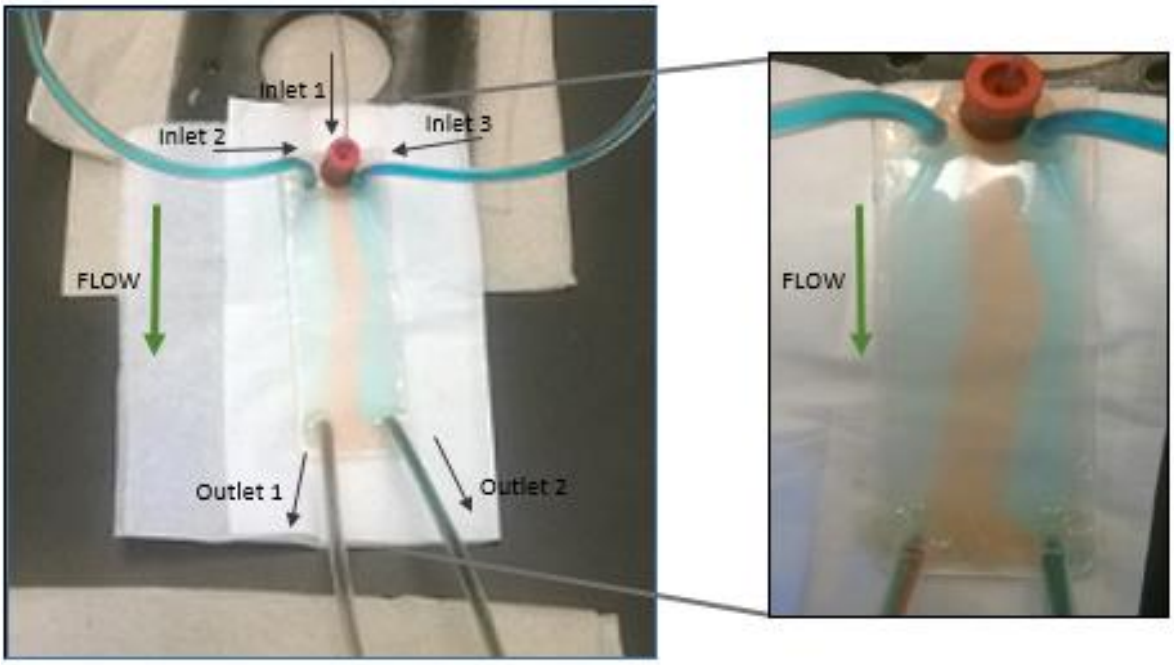

Figure 12: Experimental setup showing the flow of fluid through a Rigid Flow-through Device. The three inlets contain dye; red color represents the fluid containing particles/fluorescent beads and the blue fluorescent fluid represents a 1x solution of phosphate-buffered saline (PBS), which helps preventing false or uninteded displacement.

In order to see if the outer two inlets help the particles enter into the device in a flow-focused manner rather than flowing all across the mesh, food color and flurosecent dye were used to check to visualize the paths of fluids through the device. Figure 12 shows photographs of a Rigid Flow-through Device with dyed inlet fluids. The pinched zone of red fluid confirms that the microbeads in this fluid are being confined to the middle of the device. This allows us to determine which direction the mesh will displace the particles.

Here we are using capillary tubing and Nanoport fittings on the bead inlet (Inlet 1) to ensure that only one particle enters the device at a time and the particles do not bump into each other. Also, introducing particles in a linear manner decreases the chances of particles interacting with each other causing false/unintended displacement.

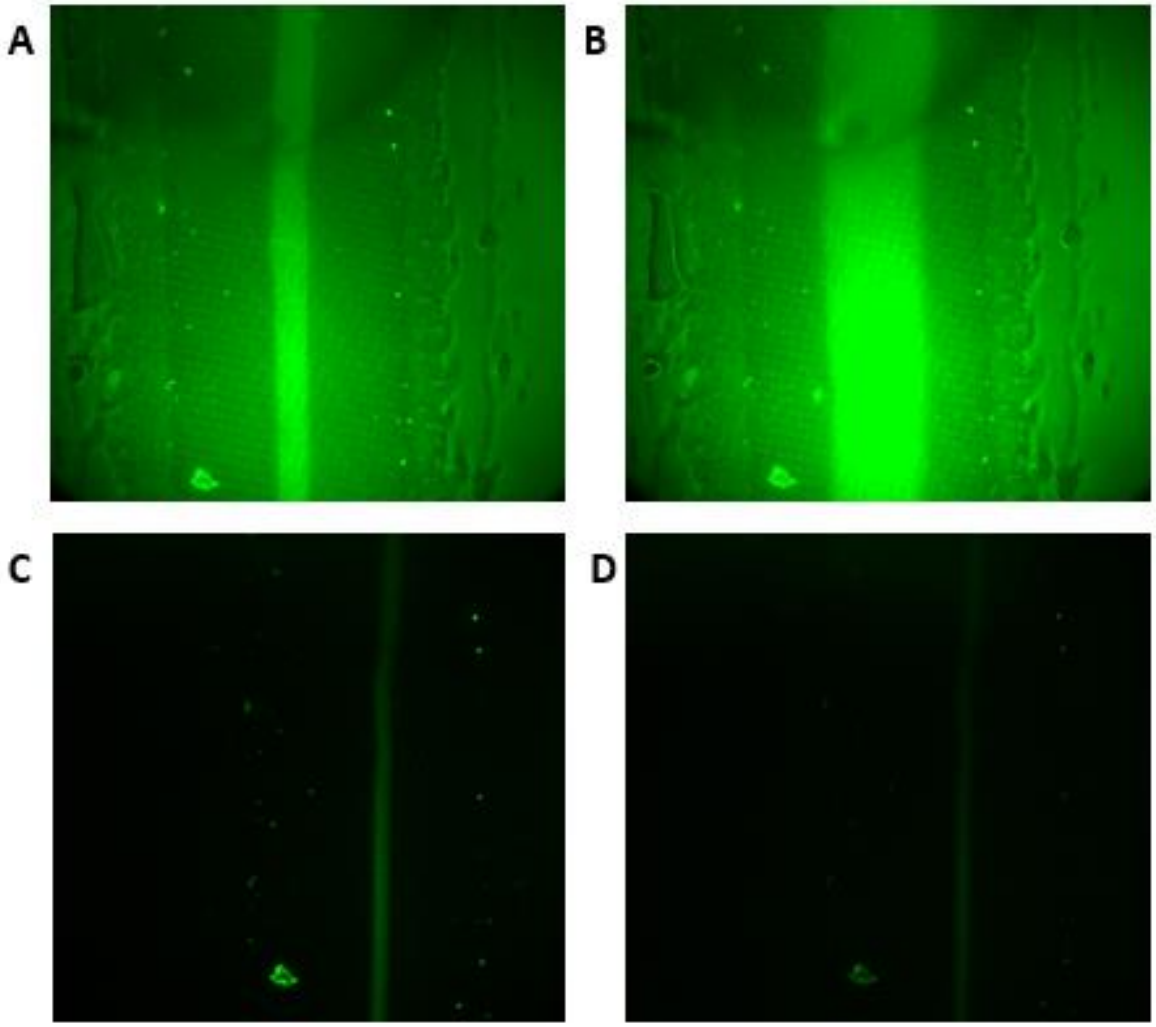

Figure 13: Fluorescent dye used to visualize the phenomena of pinched flow reducing any kind of false displacement and to see regulated flow rate

To confirm that the inlet 2 and inlet 3 are indeed decreasing the chances of unintended flow displacement, a fluorescent dye was used. The dye mixed with 1x PBS solution was pumped through Inlet 1, and Inlets 2 and 3 received degassed PBS without fluorescent dye. By adjusting the flow rate or the channel sizes, we can successfully pinch the flow containing the beads (Fig. 13 A and B). Adjusting the channel size to increase or decrease the resistance in the inlets can also cause a difference in flow rate. Fig 13 C and D shows the effect of reducing the flow rate in inlet 1 and maintaining the flow rate in inlet 2 and inlet 3.

3.4 Experimental Optimization:

We set to find a solution to different problems that are encountered while running the initial experiments. These problems include trapping of air bubbles in the devices, sticking of fluorescent beads inside the devices, and issues with vacuum-driven flow.

3.4.1 - Trapped Air Bubbles

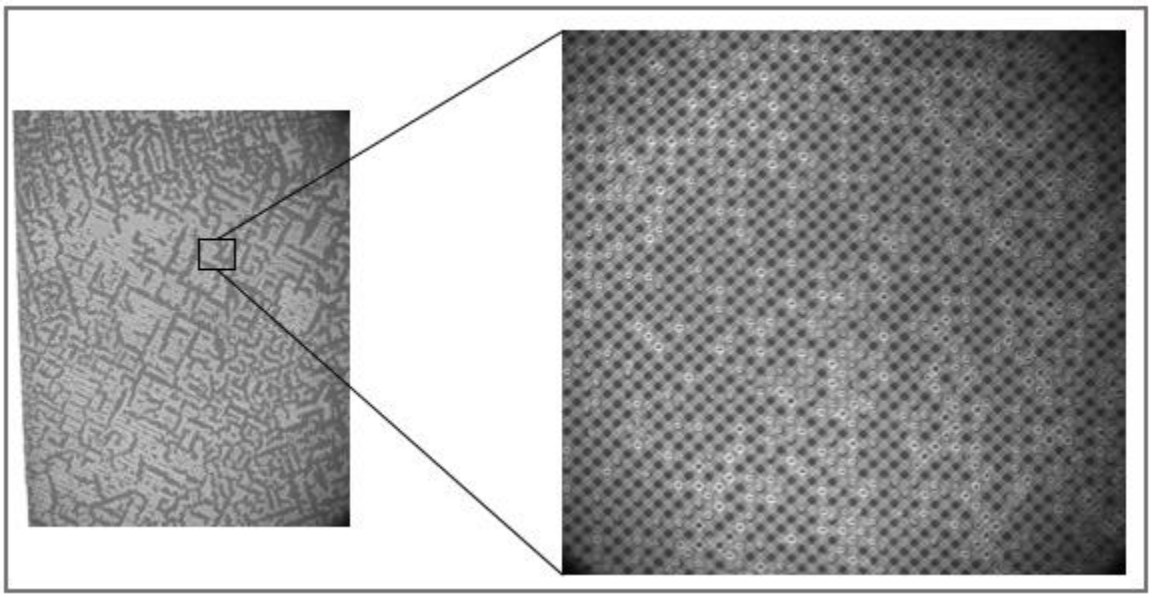

Figure 14 : Microscopic view of the device showing the air bubbles trapped in the mesh.

Air bubbles are a major cause of inconsistent and inaccurate results in microfluidics. Initially as a precaution, degassed 1x PBS water was used to prevent the trapping of air bubbles. This degassed water was treated with BSA (bovine serum albumin) and introduced into the device. Even after using degassed water and BSA, we still were facing the issue of trapped air bubbles in the mesh. We then distributed 100 ml of PBS into individual 10 mL tubes during degassing, to increase the surface area over which gas is removed from the buffer. We also eliminated BSA and TWEEN 20 from the PBS buffer.

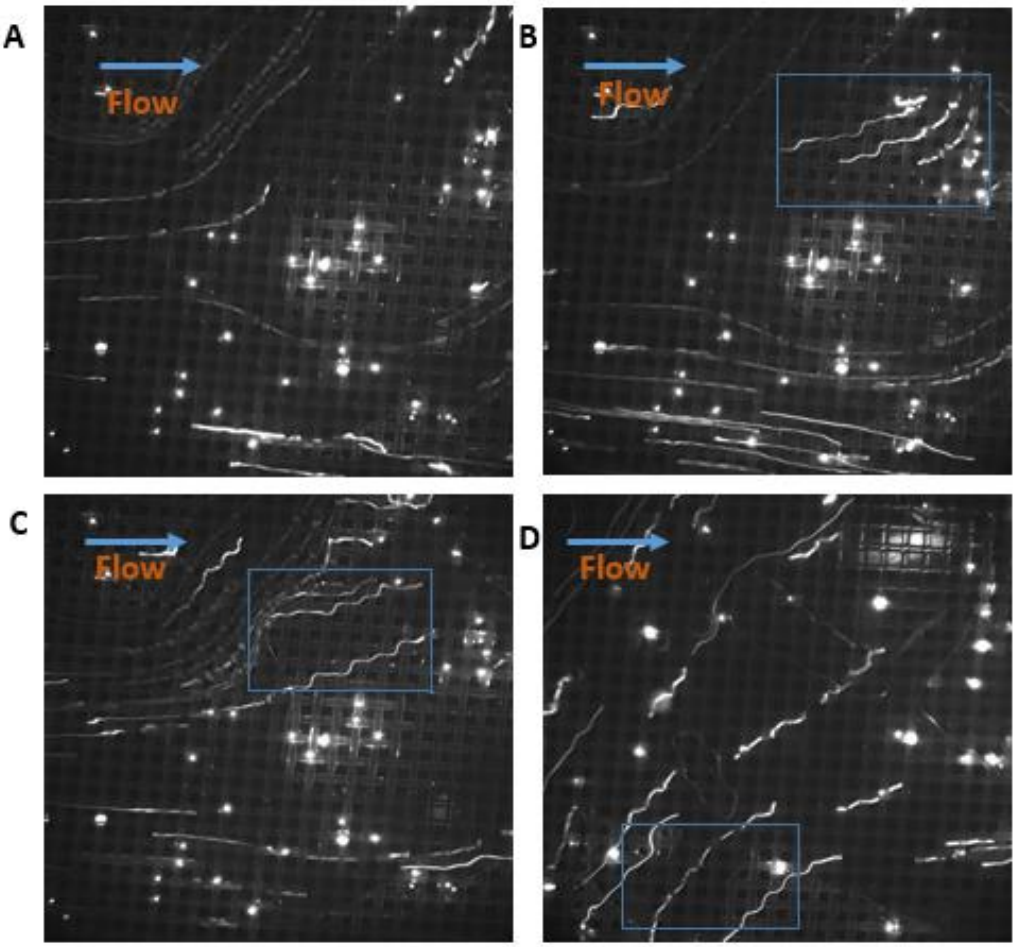

Figure 15: Microscopic view of the device showing the air/water bubbles trapped in the 78 μm mesh and its effect on the beads flowing through. The highlighted areas represent a normal interaction of beads with the mesh.

Figure 15 shows that the bubbles can affect the flow of the fluid and interaction of fluorescent beads with the mesh in a drastic way. The highlighted areas show how the 5 μm beads interact with mesh in regions without bubbles. However, in the portion of the

device with trapped bubbles, the beads tend to interact only with the water and not the mesh. In the background we can see the 10 μm beads stuck in the mesh.

3.4.2: Sticking of Beads

In our research, we are using 5 μm and 10 μm fluroscent beads for particle sorting. These sizes mimick the sizes of blood cells approximately and are under the required critical diameter. We are using 50 μm and 78 μm pore size nylon meshes, which we hypothesized would faciliate bead interactions with the mesh. Due to use of vacuum-driven head pressure flow, we observed significant sticking of beads.

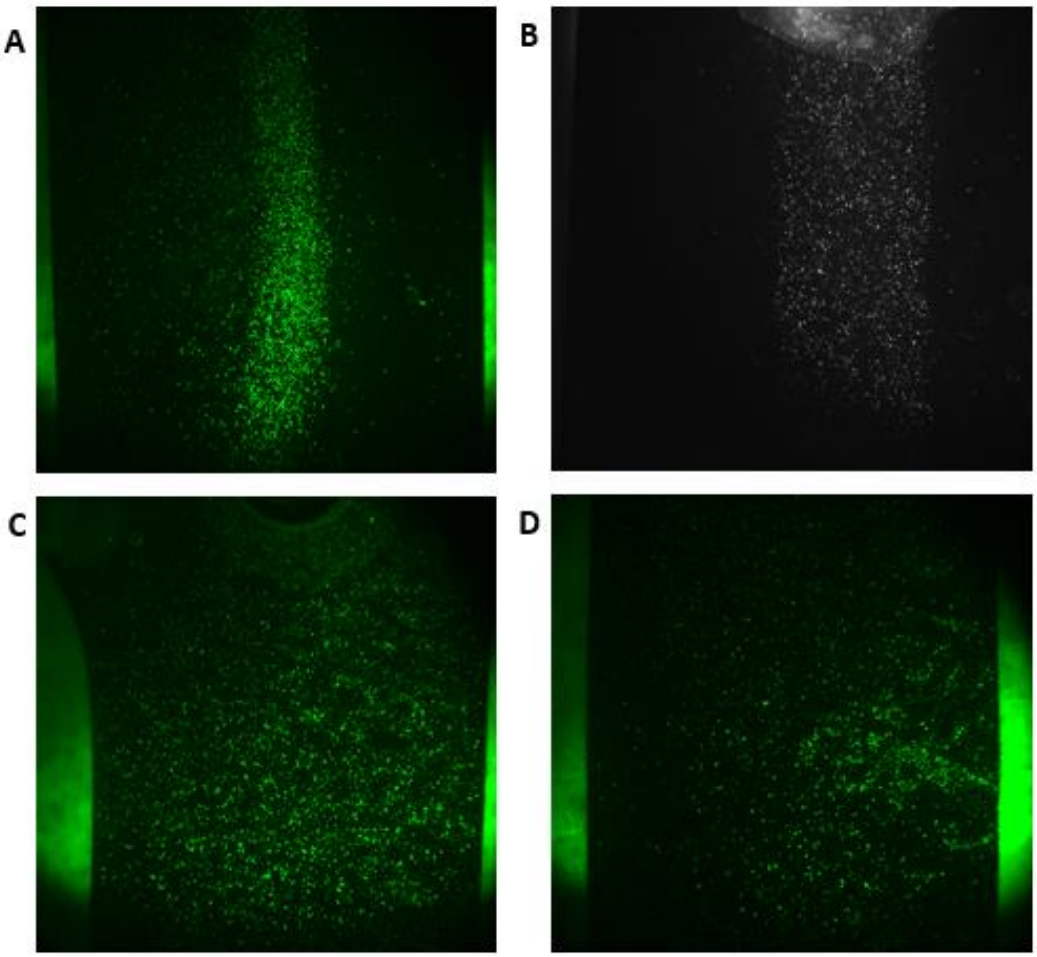

Figure 16: Microscopic view of the device showing beads trapped in the mesh.

We observed that 80% of stuck beads were due to the 10 µm beads stuck between the over-under obstacles of the mesh, while 5 µm beads were still able to interact with the mesh. **Figure 16** A and B shows the 10 µm and 5 µm beads in the channel. Figure 16 C and D shows the 10 µm stuck beads near the adapters.

3.3.3: Vacuum-driven flow

Our initial experiments were conducted using vacuum-driven pumping and head pressure and imaged using a Leica MZFLIII stereoscope. The time of exposure is more than four seconds, as a result we see more brightness from the stuck beads. We found that the use of head pressure precludes accurate measurements of the flow rate in the device.

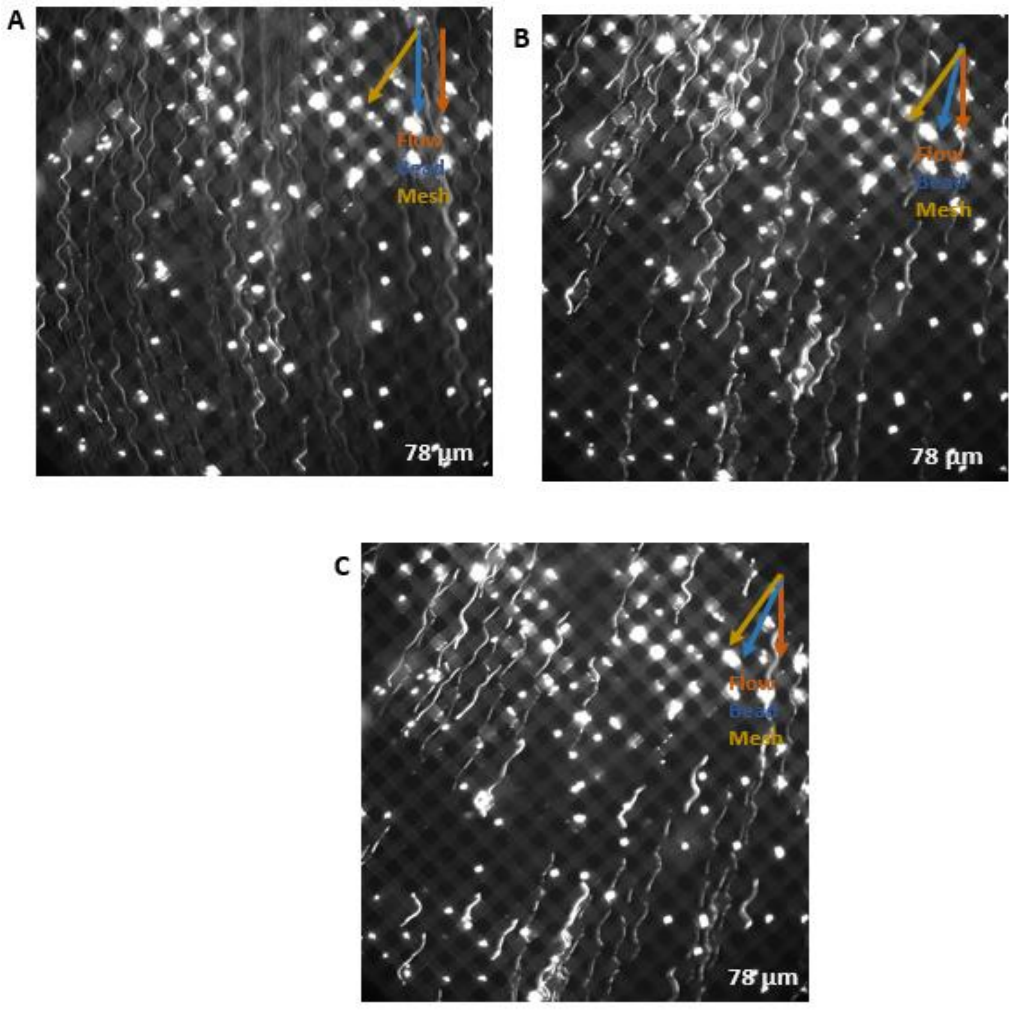

Figure 17: Microscopic view of the mesh showing the interaction of the beads affect by the vacuum driven pump. A) Vacuum driven flow of beads; B & C) Without Vacuum pressure flow of beads

While observing the results, we noted that the during vacuum-driven flow, an interaction (zigzag movement) between the mesh and the 5 μm beads was evident, but the beads nonetheless end up going straight through the device and there is no net lateral displacement (**Figure 17A**). Once the vacumm pump is switched off, a sudden change in the direction of bead movement takes place. **Figure 17 B and C** show how irrespective of the flow of the fluid, the 5 μm beads starts moving along the angle of the mesh in a manner similar to how the beads would have interacted with the obstacles in a DLD device. This result suggested that by placing the mesh at specific angles, we migh be able to separate particles by their sizes in these devices.

To reslove these issues, we switched from vacuum driven flow to the use of syringe pumps. By using syringe pumps, we could regulate the flow rate and optimize the flow of fluid in the device. We used a constant flow rate for the outer inlets and varied the flow rate of the inlet contiaining the beads. This allowed us to obtain more precise and constient results and oberve more interactions between the beads and the mesh, the results of which are discussed in the next section.

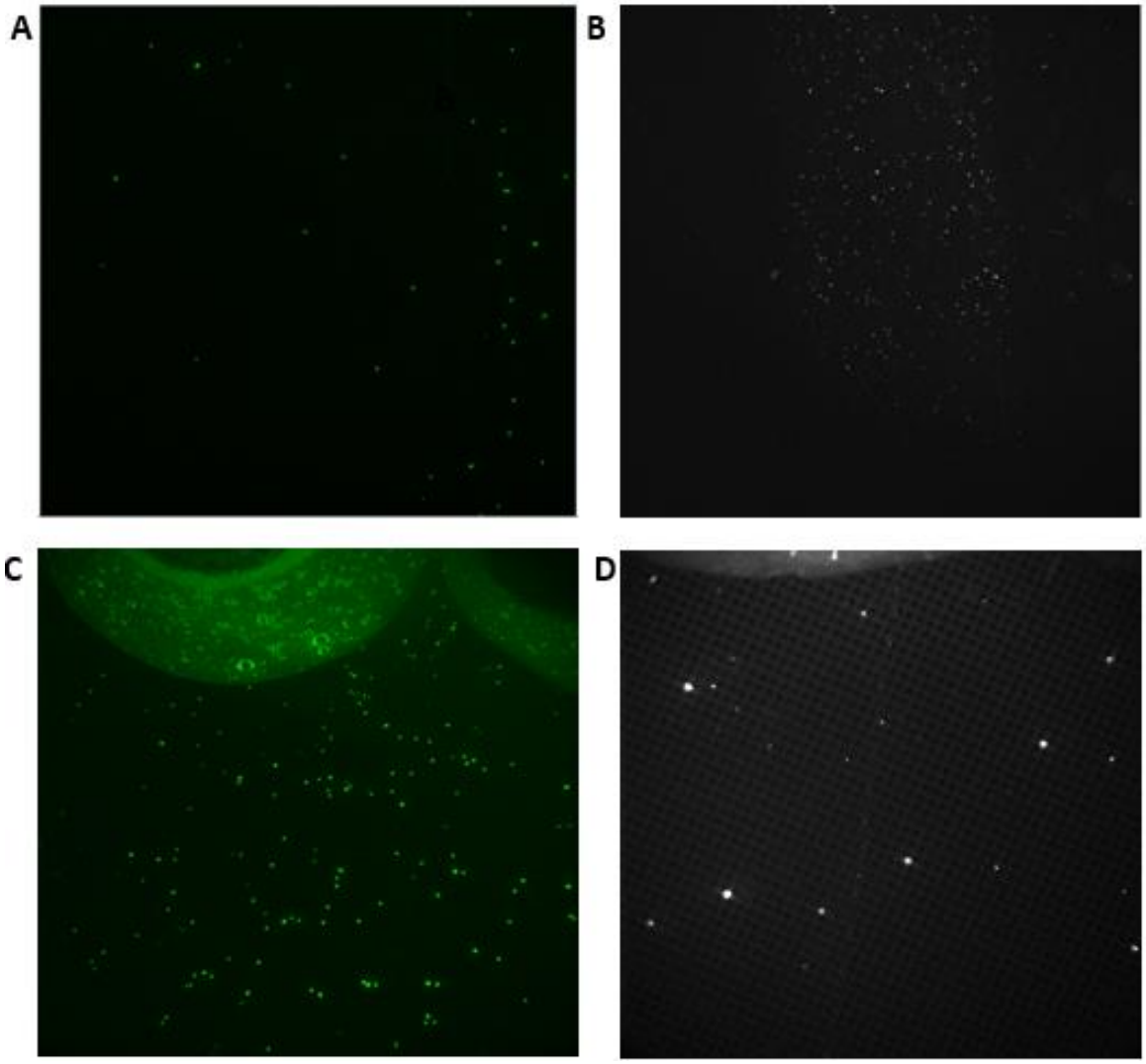

Figure 18: Images of the mesh after using syringe pumps and using fluid without BSA and Tween 20 . A&C show reduction in stuck 10 μm beads B &D show reduction in stuck 5 μm beads

Figure **18 A** is an image of the mesh showing the dramatic reduction in bead sticking after switiching to syringe pumps and eliminatin BSA and TWEEN20. There are almost no 5 μm beads and only a few 10 μm beads stuck even after a complete run on the device. Figure

18 B shows the image of the mesh at lower magnification, which makes it possible to view the full fluid channel. In comparison to Figure 15, we can see a significant reduction in the number of stuck beads. Even though we are not able to completely get rid of the sticking, they are reduced by a large scale.

Figures 18 C and D show a higher-magnification view of the device containing 10 μm and 5 μm beads, respectively. In Figure 18 C, we observe fewer stuck beads near the channel entrance compared to Figure 15. In Figure 18 D, we observe a 5 μm bead interacting with the mesh and travelling at an angle without any obstruction from air bubbles or stuck beads.

BSA and TWEEN 20 were initially included in our buffers to stop the sticking of beads and to reduce bubbles. But, as noted above, BSA and TWEEN 20 created more air bubbles and didn't help with the sticking. Only highly-degassed PBS water was used, which resulted in getting rid of bubbles along with use of syringe pumps. The flow rate of the main inlet was usually maintained with less than 0.3 ml/min and the outer inlets had a varied flow rate of less than 0.4ml/min while using syringes of 10 ml. The outlets were connected to glass vials where we could observe that the fluid coming out in both the vials was almost equal rates. This showed that fluid was flowing at a constant rate through the mesh.

3.4 Charaterization of Bead Flow in Mesh Device

While working with vaccum driven flow, we had observed the beads interact with the mesh in a zigzag manner as a particle would do in a DLD device. We also observed that at a low flow rate, the angle of the mesh can affect the direction of the flowing beads. To further explore this observation, we placed the mesh between the glass slides at different angles and visualized beads flowing through the devices. The angles that showed most deflection of the beads were 0/90 ± 5, 30 ± 5 , 45 ± 5 and 60 ± 5 degrees. The five degree uncertainty arises from making the device, when the mesh may move a little while applying epoxy or while placing the mesh between the glass slides.

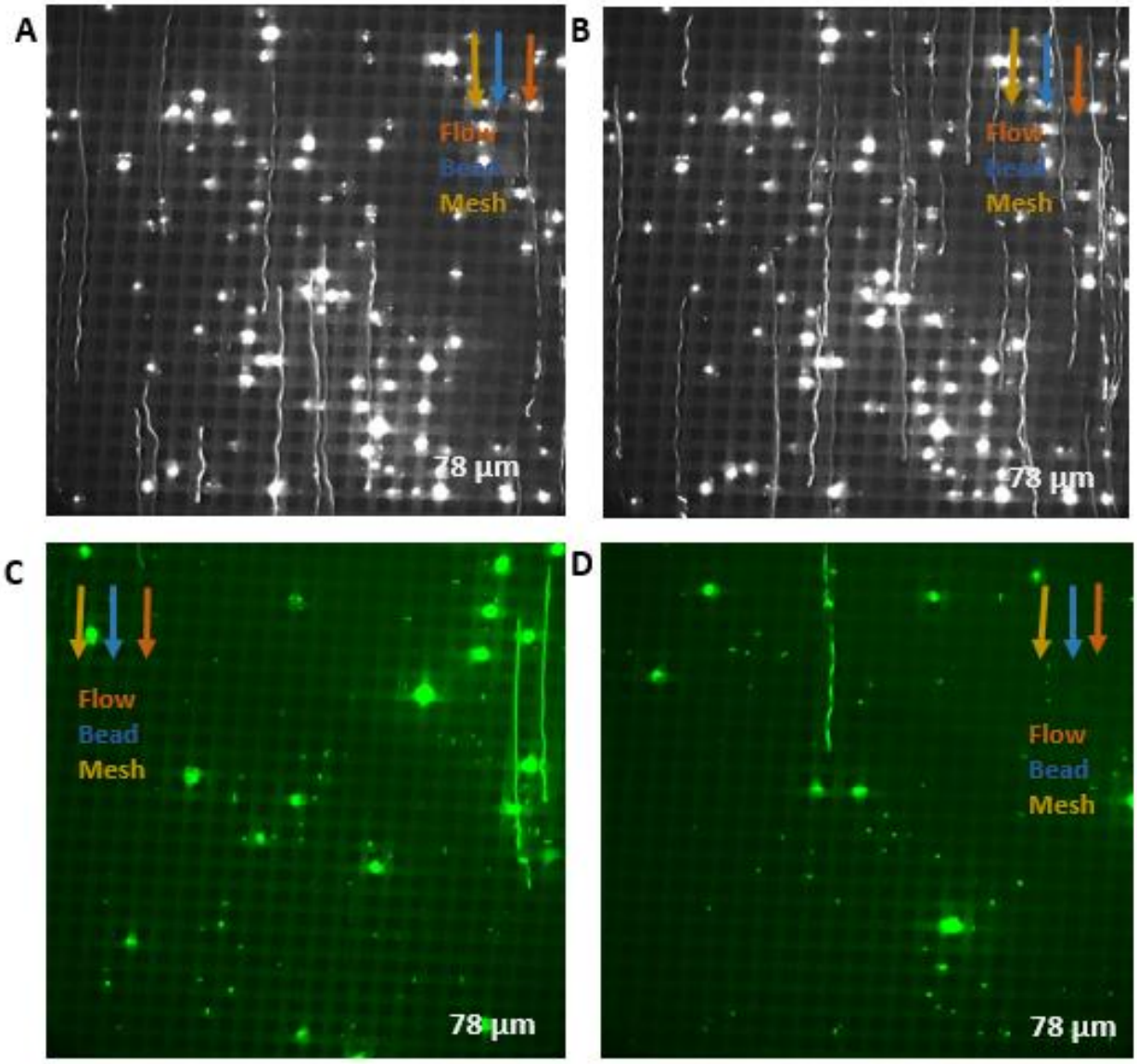

Figure 19: Images showing the flow of beads through a 0/ 90 ± 5 degree mesh.

Fgure 19 A and B show images of 5 µm beads flowing straight through a mesh at 0/90 degrees. At this angle, the presence of the mesh does not influence the flow of the beads. Similarly, in Figure 19 C and D we see that 10 µm beads flow straight with minimal zizgzag

movement. This result is similar to bead paths that would be observed in a DLD device if the obstructions were not arranged at an angle.

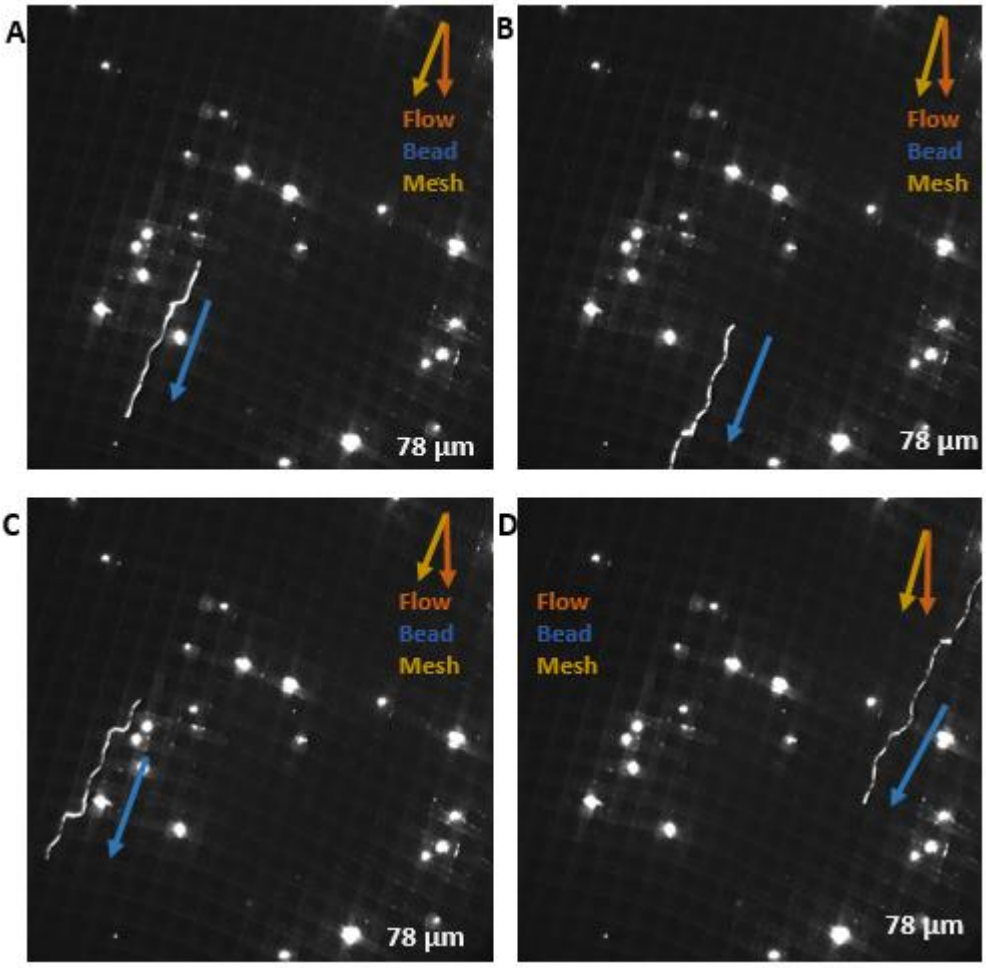

Figure 20: Images showing the flow of beads through a 40 ± 5 degree mesh.

Figure 20 shows different images of a device with 40 degree mesh, where the 5 µm beads are flowing along the angle of the mesh, even though the fluid flow is flowing straight down. The particle tends to stay in the orginal lamina moving around the mesh intersection points as would be observed in a conventional DLD device. If we treat the mesh as a normal

DLD device, the critical diameter is around 40 μm. This means that particles smaller than this size should show a zigzag motion as observed. The mesh in this device appears somewhat distorted; this rare event maybe due to epoxy moving in between the glass slides. This problem was solved by clamping the device strongly during epoxy application and curing.

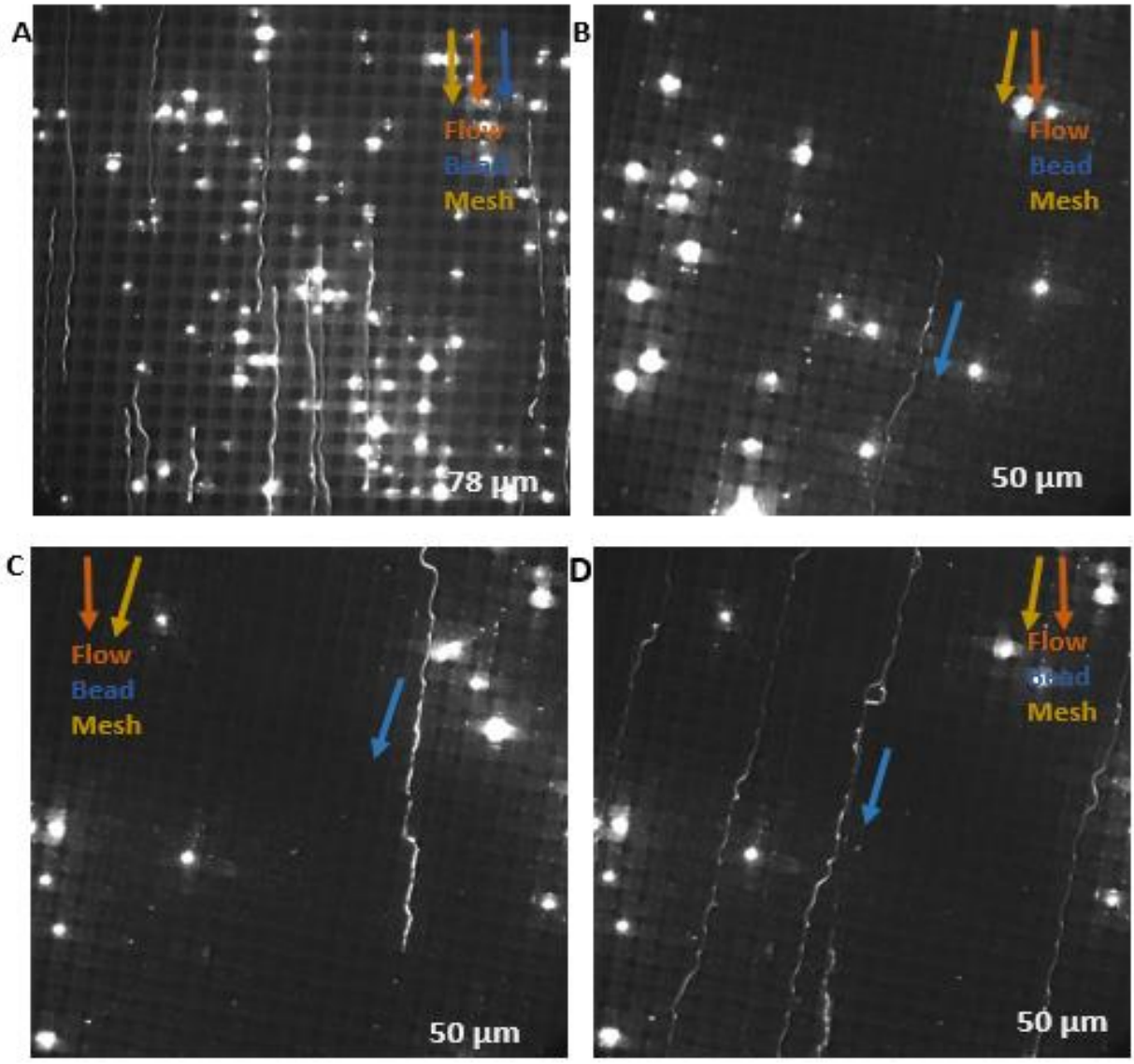

Figure 21: Images showing the flow of beads through a 30 ± 5 degree in a 50 µm mesh compared with a zero degree mesh. A) flow of beads through a 0/90 degree mesh B) Flow of beads in 50 µm mesh. The beads shows a zigzag movement and there is net lateral displacement.

Figure 21 shows the images of 5 µm beads being deflected while flowing through a 50 µm mesh

(compared with the zero degree deflection in Figure 21 A). These images were taken at a four second exposure time to enable us to obesrve beads traveling through a large part of the mesh. We do observe some stuck beads, but they do not interupt the flow of other beads. A clear zigzag movement can be seen in Figure 21 B, C, and D.

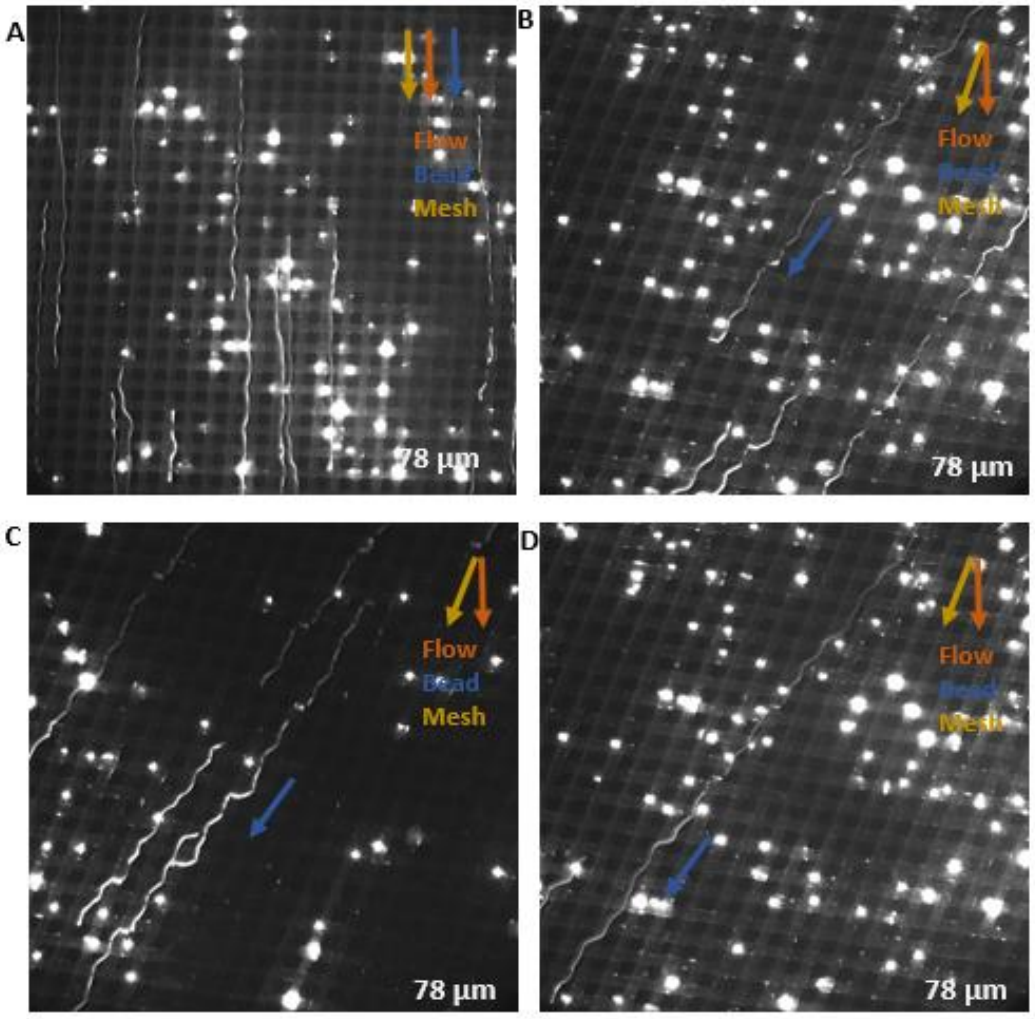

Figure 22: Images showing the flow of beads through a 60 ± 5 degree(fig 22B,C,D) in a 78 µm mesh compared with a zero degree mesh(22A).

In Figure 22, we observe that the mesh angle of 60 degrees significantly affects the trajectories of 5 μm beads. Compared to the zero degree mesh in Figure 22 A, we can clearly see the beads moving along the angle of the mesh, even though the flow is in the straight down direction. The beads follow a zigzag movement staying in the orginal lamina but moving in a direction.

3.5 Charaterization of Cell Behaviour in Mesh Devices

The last aim of our research is to observe the behavior of actual blood cells when they flow through this device. We used mouse blood and diluted it in PBS (1x) and ran it through the device using the same experimental setup with syringe pumps. Mouse blood contains 0.1 % white blood cells and 99.9 % red blood cells[7].

Figure 23 shows that the mouse blood cells demonstrate a zigzag movement along the mesh, as was observed with the beads. The cells tend to remain in their lamina. As particles, the cells also assume over-under bridge of the mesh as pillars and behave in a similar manner as in a DLD device.

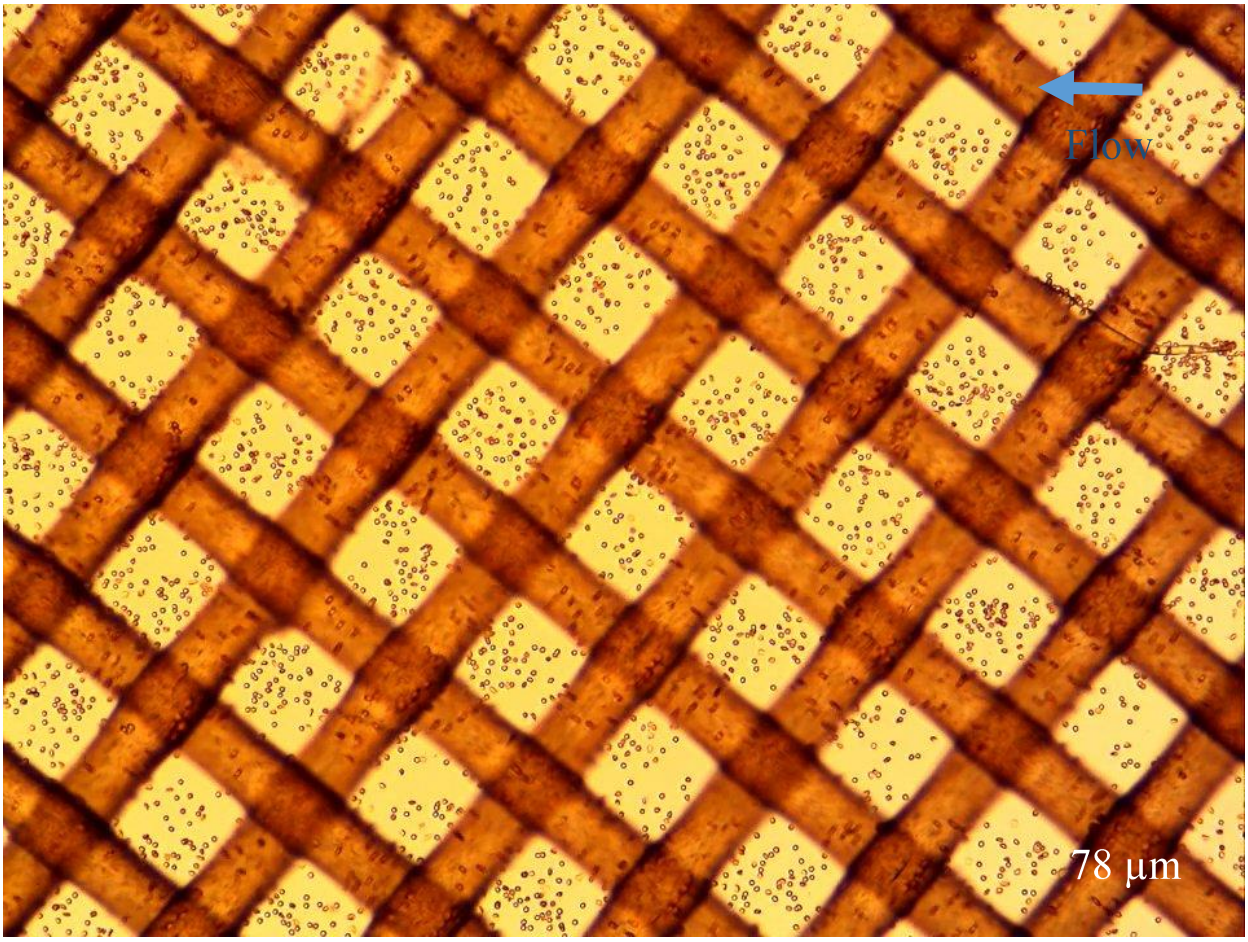

Figure 23: Image showing the flow of mouse blood cells through a 78 µm mesh oriented at a 45 degree angle.

We also observed some immobilization of cells in the over-under bridge junctions. Currently, we are not sure of the type of the immobilized cells. In future work, if the mesh can be treated with specific antibodies or the blood treated with e.g. the stain DAPI to distinguish between red blood cells and white blood cells, we might be able to identify immobilized cells or observe differences in the direction of the flow for both these types of cells [5].

Additionally, for better imaging of cells in the device, we can use a different design as shown in Figure 24. Instead of covering the top of the mesh with a thick glass slide, a cover slip can used to get a higher-magnification view of the mesh and cells.

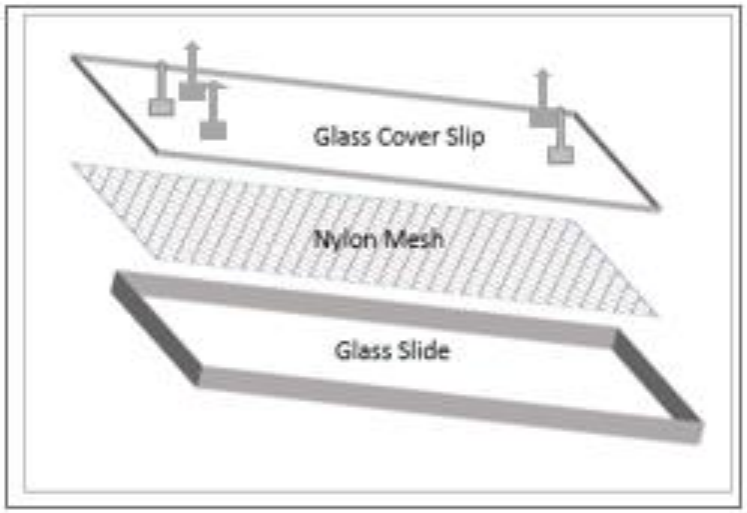

Figure 24: Utilizing a glass cover slip in the fabrication of mesh devices for enhanced optical imaging.

4 CONCLUSIONS:

The results obtained from the Rigid Flow-through Devices were very encouraging. After eliminating some of the problems faced during preliminary results like eliminating air bubbles to minimum and reducing the number of stuck beads by almost 80 percent, we obtained some promising results while using syringe pumps for regulated flow rate. The movement of particles in our mesh devices is very similar to the movement of particles in

DLD devices. As predicted, the angle of the mesh relative to the fluid flow affects the flow of particles in a significant manner, which may ultimately be used to separate particles with different sizes in the future. Even with the zigzag movement, the particles in our mesh devices demonstrate a net lateral displacement. The flow rate of the fluid needs to adjusted before it can separate cells of different sizes.

Even though we are using a larger size mesh for separating beads, we expect that a smaller size mesh might be more helpful while separating cells.

The immobilization of large size particles due to sticking can also be taken into consideration. This device can be used to capture larger size cells and allow the small size cells to pass through.

5.FUTURE WORKS:

Deterministic lateral displacement (DLD) Devices have proven to show their effectiveness in separating different types of cells. In recent studies, DLD devices have also been used to capture certain cell types. If we were to coat our the mesh with different antibodies like anti-EpCAM, the mesh might be able to capture circulating tumor cells. These devices show how particles are affected by the angle of mesh in the device; in the future this can help in separating cells from plasma in blood, or even isolating different type of cells based on their size.

REFERENCES:

1. J. P. Beech, *Microfluidic separation and analysis of biological particles,* PhD, Lund University, 2011

2. M. J. Tomlinson, S. Tomlinson, X. B. Yang and J. Kirkham, *J. Tissue Eng.*, 2013, **4**, 2041731412472690

3. Shields CW, Reyes CD, López GP. Microfluidic Cell Sorting: A Review of the Advances in the Separation of Cells from Debulking to Rare Cell Isolation. *Lab on a chip.* 2015;15(5):1230-1249. doi:10.1039/c4lc01246a.

4. Julien Autebert, Benoit Coudert, François-Clément Bidard, Jean-Yves Pierga, Stéphanie Descroix, Laurent Malaquin, Jean-Louis Viovy, Microfluidic: An innovative tool for efficient cell sorting, Methods, Volume 57, Issue 3, July 2012, Pages 297-307, ISSN 1046-2023,

5. Inglis DW, Davis JA, Austin RH, Sturm JC (2006) Critical particle size for fractioning by deterministic lateral displacement. Lab Chip 6:655-658

6. J. A. Davis. Microfluidic Separation of Blood Components Through Deterministic Lateral Displacement, Doctor of Philosophy, Princeton University, 2008.

7. Nemzek J, Bolgos G, Williams B, Remick D (2001) Differences in normal values for murine white blood cell counts and other hematological parameters based on sampling *Inflammation Research* 50(10):523–527.

8. Choi S, Park J-K. Lab Chip. 2007; 7:890. [PubMed: 17594009] Choi S, Park J-K. Small. 2009; 5:2205. [PubMed: 1963727

9. Tejas Patel ,. Cell and Particle Sorting Using Lateral Flow in Woven Meshes, University Of California,Riverside, 2014

10. Shields CW IV, Reyes CD, López GP (2015) Microfluidic cell sorting: a review of the advances in the separation of cells from debulking to rare cell isolation. Lab Chip 15:1230–1249

11. T. M. Squires and S. R. Quake, *Rev. Mod. Phys*, 2005, 77, 977-1026